

H α photometry of low mass stars in 47 Tucanae: chromospheric activity and exotica

G. Beccari^{1*} G. De Marchi² N. Panagia^{3,4,5} and L. Pasquini¹

¹European Southern Observatory, Karl-Schwarzschild-Strasse 2, 85748 Garching bei München, Germany

²ESA, Space Science Department, Keplerlaan 1, 2200 AG Noordwijk, The Netherlands

³Space Telescope Science Institute, Baltimore, MD 21218, USA

⁴INAF-CT, Osservatorio Astrofisico di Catania, Via S. Sofia 78, 95123 Catania, Italy

⁵Supernova Ltd, OYV #131, Northsound Road, Virgin Gorda, British Virgin Islands

ABSTRACT

We have used archival *Hubble Space Telescope* observations obtained with the *Advanced Camera for Surveys* to study the H α emission properties of main sequence stars in the globular cluster 47 Tucanae. Using a combination of multi-band observations in the F606W, F814W and F658N bands, we search for stars showing H α excess emission. An accurate photometric measurement of their H α equivalent width allows us to identify objects with large H α emission, which we attribute to mass accretion rather than enhanced chromospheric activity. The spatial position of some of these stars is coincident with that of known X-ray sources and their location in the colour-magnitude diagram allows us to classify them as active binaries or cataclysmic variables (CVs). We show that this method, commonly adopted to study accreting discs in young stellar objects, can be successfully used to identify and characterise candidate CVs.

Key words: Accretion, accretion discs – binaries: close – Globular Cluster : individual (47 Tucanae) – Stars: chromospheres

1 INTRODUCTION

Globular Clusters (GCs) are very efficient “kilns” for forming exotic objects, such as low-mass X-ray binaries (LMXBs), cataclysmic variables (CVs), millisecond pulsars (MSPs), and blue straggler stars (BSSs). Most of these exotica result from the evolution of binary systems originated and/or hardened by stellar interactions in the dense cluster cores, thus serving as a diagnostic of the dynamical evolution of GCs (Bailyn 1995). In particular, CVs are semi-detached binary stars, consisting of a white dwarf (WD) primary accreting from a main-sequence (MS) or a sub-giant companion (see Knigge et al. 2011, for a recent review) while LMXBs and MSPs contain a neutron star (NS).

The accretion process leaves some characteristic signatures in the spectrum of these stellar exotica. For instance, a typical feature observed in the spectra of CVs is emission from Balmer recombination lines (e.g. H α , H β ; see Witham et al. 2006) or excess in the ultraviolet (UV) continuum (see e.g. Ferraro et al. 2001). Williams (1983) suggest that an accretion disc is the dominant source of optical and UV emission, whereas line emission may originate from the outer edge of the disc or the accretion corona. In magnetic CVs, optical and UV emission likely generate from accreted material that flows along magnetic field lines, and accretes directly onto the WD at/near its magnetic poles without forming a viscous disc. How-

ever, UV and line emission also originates from various parts of an accretion disc in non-magnetic or only weakly magnetic CVs (see e.g. Witham et al. 2006).

A different source of emission lines in the spectra of MS stars is chromospheric activity (CA), due to processes that make the temperature of the outer atmosphere higher than it would be if radiative equilibrium held. Such non-radiative heating mechanisms are powered by convection and magnetic fields. In the outer layers of these stars, the temperature is increasing towards the surface, and the main cooling mechanism is radiative loss through strong resonance lines, such as Ca II H and K, Mg II h and k, H α (Linsky 1980). Signatures of H α emission from CA in spectra of low mass stars are thus expected and a detailed knowledge of the H α equivalent width (hereafter EW(H α)) produced by CA is crucial when searching for H α emission signatures from accreting stars of all ages.

A number of studies have looked for accreting binaries through emission lines searches in GCs (e.g. Pooley et al. 2002; Kong et al. 2006; Bassa et al. 2008; Cohn et al. 2010; Lu et al. 2011). The GC 47 Tucanae is definitely one of the most promising targets for this kind of investigation, since it harbours a crowded zoo of stellar exotica, including BSSs, LMXBs and candidate CVs (e.g. Ferraro et al. 2001). Heinke et al. (2005, hereafter H05) published a catalogue of 300 X-ray sources inside the half-mass radius of 47 Tuc ($r_h = 3.17$; Harris 1996) obtained from deep X-ray observations with the *Chandra X-ray Observatory*. Many

* E-mail: gbeccari@eso.org

Table 1. Log of the observations

Filter	N. of exposures	Tot. exposure time	Prop. ID	Date of obs.
F606W	4	200s	10775	13.03.2006
F814W	4	200s	10775	–
F658N	7	2630s	9281	30.09.2002
F658N	7	2630s	9281	02.10.2002
F658N	6	2180s	9281	11.10.2002

of these stars are classified as CVs, interactive binaries, quiescent LMXBs (qLMXBs) and MSPs, and therefore a signature of $H\alpha$ excess emission should be expected for at least some of them. Recently Knigge et al. (2008) presented far-UV spectroscopic observations obtained with the *Hubble Space Telescope* (HST) of 48 blue objects in the core of 47 Tuc. These authors provide spectroscopic confirmation of 3 CVs via the detection of emission lines and find new evidence for dwarf nova eruptions from two of them. However, a large number of objects in the H05 catalogue still remain unclassified.

Following a method presented by De Marchi et al. (2010, hereafter DM10) to detect and study stars with $H\alpha$ excess emission in star forming regions, we have used archival HST observations acquired with the *Advanced Camera for Surveys* (ACS) to perform an $H\alpha$ survey of MS stars in 47 Tuc. The method of DM10 uses a combination of V and I broad-band photometry with narrow-band $H\alpha$ imaging to measure the $EW(H\alpha)$ of stars showing $H\alpha$ excess emission, thereby offering a new and very efficient way to identify and characterise accreting stars in GCs. In this work we present the method and we explore the possibilities offered by its application to 47Tuc.

In Section 2 we describe the dataset and the reduction strategy while the DM10 method is described in Section 3. We applied the method of DM10 with two main goals. Firstly, we searched for $H\alpha$ excess emitters amongst the cluster stars located at a radius $r > 70''$, where the photometric completeness allows us to perform a homogeneous $H\alpha$ survey of all the spectral types sampled by our data (Section 4). Secondly (see Section 5), we searched for optical counterparts to the H05 X-ray sources by looking for objects with $H\alpha$ excess emission inside the X-ray error circle, regardless of their location in the cluster. In Section 6 we conclude by discussing the possible nature of some unclassified objects from their location in the colour-magnitude diagram (CMD) of the cluster.

2 OBSERVATIONS AND DATA REDUCTION

The data used in this work consist of a series of archival HST/ACS images obtained through the broad F606W and F814W bands and with the narrow-band F658N filter (hereafter V, I and $H\alpha$, respectively). The images, acquired with the ACS in the Wide Field Channel (WFC) mode, cover a total field of view (FoV) of $\sim 3'.4 \times 3'.4$ with a plate-scale of $0''.05$ per pixel. The V- and I-band observations come from proposal 10775 while the $H\alpha$ band data belong to the HST proposal 9281. Details on exposure time for each filter are given in Table 1. The images sample the cluster centre, but slightly different pointings and telescope orientations have been used to perform these observations. As a consequence, the sampled area in common between the two datasets is $\sim 40\%$ less than the whole FoV. The geometry of the FoV of the combined datasets is shown in Figure 1.

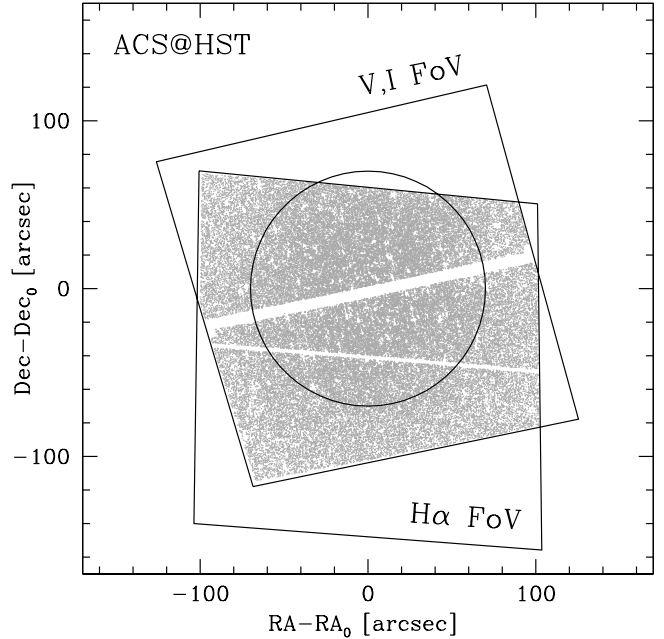


Figure 1. Map of the combined ACS observations. The position of the stars are plotted with respect to the centre of gravity from Ferraro et al. (2004). The images in the inner $70''$ from the cluster centre (circle) suffer from strong crowding.

2.1 Photometry of the V and I band data set

The V- and I-band images were analysed using the standard DAOPHOTII (Stetson 1987) point spread function (PSF) photometric reduction procedure. More than 50 isolated and well sampled stars were used on each flat-fielded (FLT) image¹ to accurately calculate a PSF model. PSF fitting was performed on every image with the DAOPHOTII/ALLSTAR routine and a master list was obtained which contains all objects that have been detected in at least three of the four individual exposures in each of the V and I bands. The instrumental magnitudes were then calibrated and brought to the VEGAMAG photometric system using the procedure described in Sirianni et al. (2005). A sample of bright isolated stars has been used to transform the instrumental magnitudes to a fixed aperture of $0''.5$, and the extrapolation to infinite and transformation into the VEGAMAG photometric system was performed using the updated values listed in Tables 5 and 10 of Sirianni et al. (2005)².

The final catalogue contains about 100 000 stars, sampling the MS stars down to 6.5 mag below the turn off (TO). The CMD of the stars detected in the V and I bands is shown in Figure 2. Cluster stars are shown as grey points, while the location of the MS mean ridge line obtained with a second order polynomial interpolation with a 2.5 sigma rejection, is displayed as a black solid line together with the average deviation (horizontal error bars in the plot). Finally, we used ~ 3000 stars in common with a ground based catalogue obtained with the Wide Field Imager at the MPE-2.2m tele-

¹ The FLT images were corrected for geometric distortions and for the effective area of each pixel following the approach described in Sirianni et al. (2005). Correction for losses of Charge Transfer Efficiency was performed on the FLT images following Anderson & Bedin (2010)

² The new values are available at the STScI web pages: <http://www.stsci.edu/hst/acs/analysis/zeropoints>

scope, published by Ferraro et al. (2004) to derive an astrometric solution and obtain the absolute right ascension (RA) and declination (Dec) positions of the stars sampled in the ACS catalogue. The astrometric coordinates of the stars in the WFI catalogue were registered with the ICRS reference system adopting a GCS2.2 catalogue of astrometric standards. The r.m.s. scatter of the final solution was $\sim 0''.3$ in both RA and Dec.

2.2 Photometry of the H α band data set

A different approach was used for the H α dataset. Three drizzled (DRZ) images, generated by the standard pre-reduction pipeline using the IRAF *multidriz* package, were retrieved from the HST archive. The DRZ images are a combination of 7, 7 and 6 FLT images, for an effective total exposure time of 2630 s, 2630 s and 2180 s, respectively (see also Table 1). Besides being cleaned from cosmic rays and detector imperfections, the DRZ images offer higher signal-to-noise ratio compared to the single FLT exposures and therefore a more precise measure of the H α magnitudes.

The H α images are affected by very low crowding conditions. This allowed us to safely use aperture photometry to measure the stellar magnitudes in the H α band. Moreover, as documented in the MULTIDRIZZLE Handbook, the distortion present in the imaging instruments on board HST produces sampling patterns that are not uniform across the field, due to the changing pixel size. This may cause a “blurring” in the PSF of the stars in the processed images and directly impacts the uniformity of the output PSF, making the PSF modelling in DRZ images slightly more complicated than in the FLT images.

We performed aperture photometry with the IRAF *phot* task on each DRZ image using as input coordinates the positions of the stars in the master list obtained in the V and I bands, after registering the coordinate system of each DRZ image. In order to do that a preliminary aperture photometry was performed on the DRZ images with the SExtractor photometric package (Bertin & Arnouts 1996) with the aim of producing a list of centroid and magnitudes of the stars in the three H α frames. These lists of stars were used as reference to accurately transform the coordinates of all the stars in the V and I master list onto each DRZ frame position. Cross-correlations of the catalogues were performed with CataXcorr, a code developed and maintained by Paolo Montegriffo at INAF-Bologna Astronomical Observatory (see e.g. Ferraro et al. 2004). More than 20000 stars in common between the V and I master list and each DRZ star lists from aperture photometry allowed us to reduce the uncertainties (i.e. the X and Y r.m.s.) of the transformations to $\sim 4 \times 10^{-6}$ pix.

The H α magnitudes of the stars were measured inside a radius of 2 pixels, while the background was locally estimated inside an annulus between 4 and 7 pixel radius around each star. The photometric uncertainty is defined as the standard deviation of three independent measurements of the same object. The H α instrumental magnitudes obtained in this way were finally calibrated to the VEGAMAG photometric system following the procedure of Sirianni et al. (2005).

3 SELECTION OF OBJECTS WITH H α EXCESS EMISSION

As mentioned in the introduction, our first goal is to apply the method developed by DM10 to perform a systematic and homogeneous search for candidate H α excess emitters along the cluster

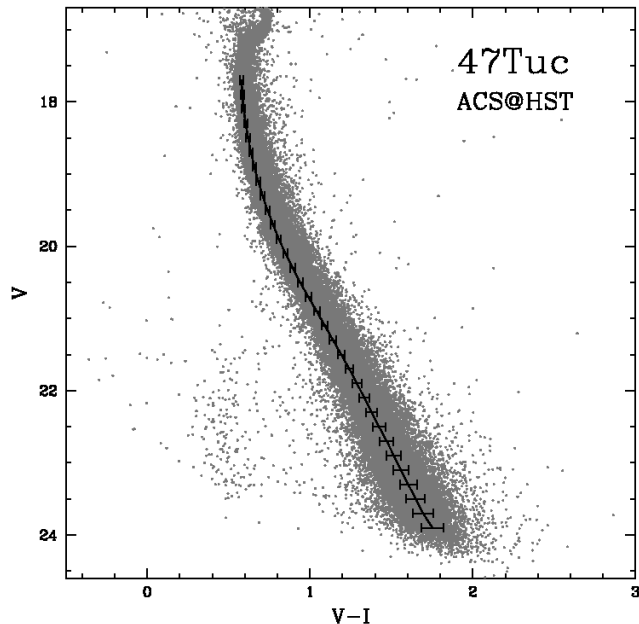


Figure 2. CMD of the ~ 100000 stars sampled in the V and I data-set of 47Tuc. The MS ridge-line is shown as a solid line, together with the average deviation (horizontal error bars in the plot). The solid line is not centred because of binaries and blends.

MS. As mentioned in the previous section, we have obtained H α magnitudes for all the objects sampled in the V and I band images. However, crowding conditions vary considerably across the field covered by our observations and the homogenous search for stars with H α excess emission is harder to achieve in the most central regions of the cluster. Therefore, in this first part of the paper (Sections 3 and 4) we study the stars located at a distance larger than $70''$ from the cluster centre (black circle in Figure 1), a region which is not affected by stellar crowding. Stars with H α excess in the central cluster regions are discussed in Section 5. We refer to DM10 (see also Spezzi et al. 2012) for a detailed description of the method, while here we illustrate the crucial steps needed to successfully apply it.

The first step consists in correcting the stellar magnitudes for reddening, which we perform by assuming the canonical extinction value towards 47 Tuc, namely $E(B - V) = 0.04$ (Harris 1996) using the Cardelli et al. (1989) extinction law with $R_V = 3.1$. It is important to clarify here that, while reddening correction might be a rather complex step when studying star-forming regions, where stars are still embedded in the molecular cloud that may cause strong differential extinction, this is not at all an issue in a GC where the stars are subject to very little or no differential reddening. In particular, giving the small amount of total reddening affecting the stars in 47 Tuc, differential reddening is rather unlikely (see Anderson et al. 2009). Moreover, in Beccari et al. (2010) we demonstrated that even over/underestimating $E(V - I)$ by much as 0.2 mag, by far larger than the uncertainty of our assumption on the reddening, would not change significantly the selection of stars with H α excess emission.

Once the magnitudes of the stars are corrected for reddening, the selection of the objects with H α excess emission is performed in the $(V - H\alpha)_0$ vs. $(V - I)_0$ colour-colour diagram, as shown in Figure 3. The traditional approach to search for sources with H α

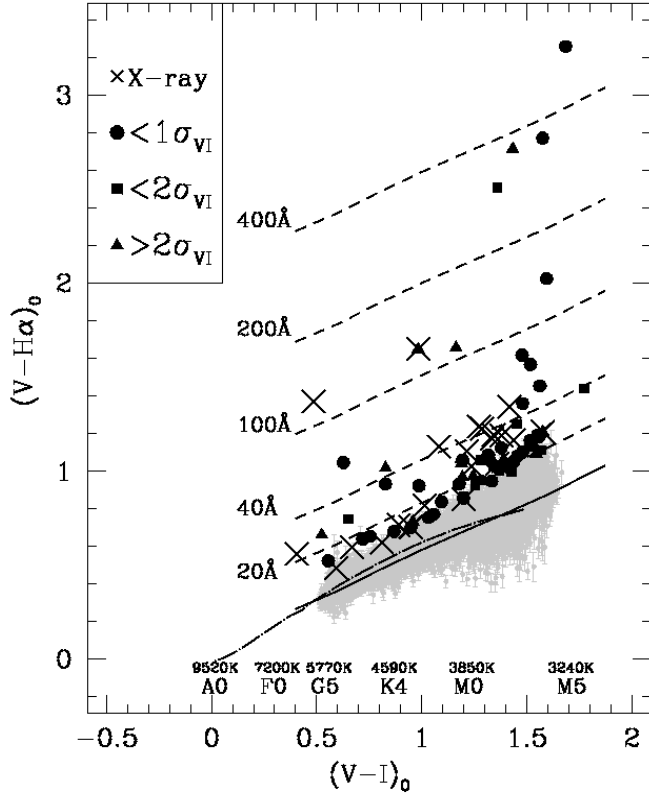


Figure 3. Selection of stars with $H\alpha$ excess emission in a colour-colour diagram. The solid line represents the median $(V-H\alpha)_0$ color of stars with an error on $(V-H\alpha)_0 < 0.1$, and is defined as the locus of stars without $H\alpha$ excess emission and hence the location of stars with $EW(H\alpha)=0$. Dashed lines show the position of stars at increasing levels of $H\alpha$ emission. All the objects with $H\alpha$ excess emission at least 5 times larger than the photometric uncertainty on their $V-H\alpha$ colours are shown in black. X-ray sources showing $H\alpha$ excess emission are shown as crosses, while solid circles, squares and triangles indicate $H\alpha$ excess emitters lying on the CMD at $(V-I)_0$ distance from the MS mean-ridge line, 1, 2 or more than 2 times the combined photometric uncertainty on the colour. The dot-dashed line shows the location of the colour relationship derived for these bands using the Bessell et al. (1998) atmospheric models.

excess is based on the use of the R-band magnitude as an indicator of the level of the photospheric continuum near the $H\alpha$ line, so that stars with strong $H\alpha$ emission will have a large $R-H\alpha$ colour (see e.g. Baily et al. 1996; Witham et al. 2006; Pallanca et al. 2010). However, as discussed in DM10, since the R band is over an order of magnitude wider than the $H\alpha$ filter, the $R-H\alpha$ colour does not provide a direct measurement of the $H\alpha$ equivalent width $EW(H\alpha)$. Conversely, an accurate determination of the continuum is obtained using the V, I and $H\alpha$ magnitudes combination shown in Figure 3, because the contribution of the $H\alpha$ line to the V and I magnitudes is completely negligible. Therefore the value of the $EW(H\alpha)$ can be directly derived. The $(V-I)_0$ colour is in addition a useful colour index for temperature determination and its use allows one to take into account the variation of the stellar continuum below the $H\alpha$ line at different spectral types. The effective temperatures and spectral types shown in Figure 3, are obtained adopting the atmospheric model of Bessell et al. (1998) and the specific ACS filters used in this investigation. As a reference, a star with an effective temperature of ~ 4800 K has colour $F555W-F814W = 1$

and $F606W-F814W = 0.78$. The latter is the filter pair used in our photometry.

Note that, while the observations in the V and I bands are simultaneous, those in the $H\alpha$ band were collected at a different epoch. Therefore, if there is variability in the continuum, the true $V-H\alpha$ values could be slightly different from those shown in Figure 3. However, Edmonds et al. (2003b) show that the magnitude of the majority of stars in this field varies by ~ 0.02 mag. This level of variability in the continuum does not affect our selection of bona-fide $H\alpha$ excess objects.

The reference line (solid line in Figure 3) with respect to which the $H\alpha$ excess emission is measured is empirically defined as the median $(V-H\alpha)_0$ colour of stars with combined photometric errors smaller than 0.1 mag (grey points in Figure 3). Note that our empirical determination agrees very well with the colour relationship derived for these bands using the Bessell et al. (1998) atmospheric models (dot-dashed line in Figure 3). Since the contribution of the $H\alpha$ line to the V magnitude is completely negligible, the $H\alpha$ excess emission can be simply obtained as the distance $\Delta H\alpha$ of a star from the empirical line, along the $(V-H\alpha)_0$ axis at the same $(V-I)_0$ colour. We consider as objects with bona-fide excess emission only stars showing a $\Delta H\alpha$ at least value 5 times larger than their combined photometric uncertainties in the V and $H\alpha$ bands ($\sigma_{VH\alpha}$).

As already mentioned, the V and I deep images are strongly affected by saturation of the bright giants, which produce diffraction spikes on the images (e.g. see Anderson et al. 2009). This implies that the magnitude of a star falling on the spikes cannot be trusted because of the uncertainty in the background estimation. We visually inspected all the candidate stars with $H\alpha$ emission and decided to conservatively discard a star if a spike was falling inside the annulus around the stellar centroid adopted for the local estimate of the background (7 pixels).

Once the $\Delta H\alpha$ value is calculated as explained above, the equivalent width $EW(H\alpha)$ for each star can be derived as $EW(H\alpha) = RW \times [1 - 10^{-0.4 \times \Delta H\alpha}]$ (see Equation 4 in DM10) where RW is the rectangular width in Å of the filter, which depends on the specific characteristics of the filter (see Table 4 in DM10).

A total of 59 stars outside of $70''$ from the cluster centre are found to have $H\alpha$ excess emission. They are marked with black symbols in Figure 3, while the coordinates and magnitudes of these objects, together with the value of $EW(H\alpha)$, are listed in Table 2. Thick dots in Figure 3 denote $H\alpha$ -excess stars with a colour distance $\Delta(V-I)_0$ from the MS mean ridge line in Figure 2 equal to, or smaller than, the photometric uncertainty on their color σ_{VI} ($\Delta(V-I)_0 \leq \sigma_{VI}$), squares denote $H\alpha$ -excess stars with $\sigma_{VI} < \Delta(V-I)_0 \leq 2\sigma_{VI}$, and triangles correspond to $H\alpha$ -excess stars with a colour distance $> 2\sigma_{VI}$. This is a simplified way to indicate the probability that a star falls on the MS, since the larger is the colour distance the lower the probability of being a single MS star.

The dashed lines in Figure 3 correspond to $EW(H\alpha)$ thresholds of 20, 40, 100, 200 and 400\AA . Notice that we are assuming a feature with positive EW as being in emission and negative EW as being in absorption. As expected, the majority of cluster stars show very low or no $H\alpha$ emission. Only 12 stars with spectral type between F0 and M0 show $EW(H\alpha) > 20\text{\AA}$. The number of objects with $H\alpha$ excess emission increases at later spectral types, but still only $\sim 0.2\%$ of the total number of objects sampled in this area show excess emission with $EW(H\alpha) > 20\text{\AA}$. The distribution of these stars in the cluster CMD will allow us to investigate more precisely the nature of these objects (see Section 6).

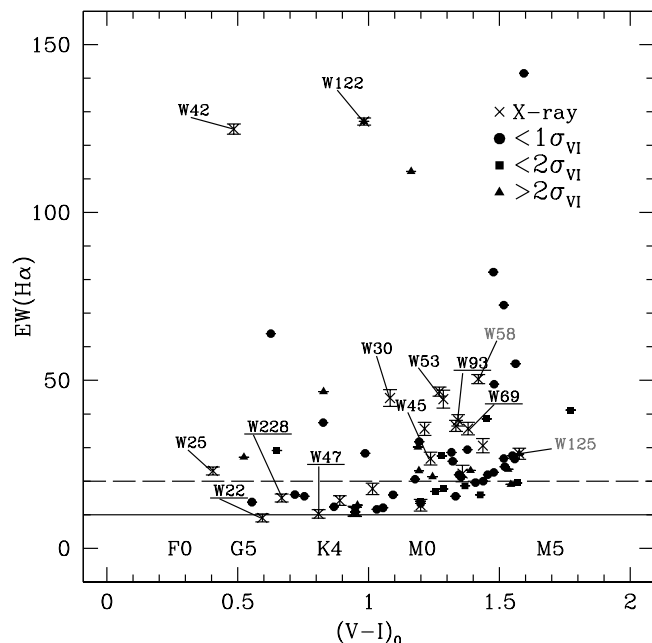


Figure 4. Distribution of $EW(H\alpha)$ for stars with $H\alpha$ excess emission as a function of their $(V - I)_0$ colour. Symbols are the same as in Figure 3. The 6 known CVs (black characters), the 5 known active binaries (ABs; underlined characters) and the 2 known qLMXBs (grey characters) are explicitly labelled in the CMD. Spectral types are also indicated. Note that error-bars are not shown because they are comparable to or smaller than the symbols.

In Figure 4, we show the distribution of the measured $EW(H\alpha)$ for all stars with $H\alpha$ excess emission detected in 47 Tuc at $70''$ from the cluster centre, as a function of their $(V - I)_0$ colour and spectral type (the latter has been computed using the models of Bessel et al. 1998). The symbols are the same as in Figure 3. It is important to notice that all the stars selected as bona-fide $H\alpha$ excess emitters show an $EW(H\alpha) \geq 10 \text{ \AA}$. This is a consequence of the selection criteria and of the quality of the data. In fact, because of the photometric quality of the data-set, only stars with an $H\alpha$ excess with a $EW(H\alpha) \geq 10 \text{ \AA}$ fulfil the requirement that $\Delta H\alpha \geq 5 \times \sigma_{VH\alpha}$.

In the following section we investigate the possibility that such a strong emission would come from pure CA.

4 CONSTRAINTS ON STELLAR CHROMOSPHERIC ACTIVITY

The $H\alpha$ spectral line has been frequently used together with the CaII K line as a diagnostic of CA (e.g. Pasquini & Pallavicini 1991). As an example, Kafka & Honeycutt (2006) published a comparison of the $H\alpha$ strengths with $V - I$ photometric colours of eight clusters and detected a dependence on cluster age of the location along the MS for the onset of CA, confirming that the colour at which activity becomes important is approximately a linear function of the logarithm of the age (see also Hawley et al. 2000). Zhao et al. (2011) demonstrate that, in general, CA decays with age from 50 Myr to at least 8 Gyr for stars with spectral types later than K5 and Lyra & Porto de Mello (2005) confirmed that the CA of dwarfs decreases with age and remains flat in a range of ages from 2 Gyr up to 11 Gyr (see their figure 10). It is important to notice that the same authors suggest that, at a given age, CA

of dwarfs increases with metallicity while, when measured through the $H\alpha$ emission, it appears to be insensitive to the activity cycle and rotational modulation.

Furthermore, as shown by Kafka & Honeycutt (2006) (see their Figures 13 – 15), it appears that no $H\alpha$ emission with $EW \geq 10 \text{ \AA}$ is measured from CA for stars of spectral type K7 or earlier. The work of Kafka & Honeycutt (2006) indicates that very few stars show $H\alpha$ emission with $EW \geq 10 \text{ \AA}$ at later spectral types. Schmidt et al. (2007) show that the CA of late-M (later than M7) dwarfs and L dwarfs can be measured as an $H\alpha$ emission of $EW(H\alpha) > 10 \text{ \AA}$. Notice that these spectral classes are not covered by our observations (see Figure 3).

We shall notice that most of the CA studies refer to pop I stars close to solar metallicity. 47Tuc is relatively metal poor and not many studies have been performed so far about CA in metal poor MS stars. A few active metal poor binaries have been studied by Pasquini & Lindgren (1994). They find that the $H\alpha$ emission, used as indication of CA, is observed in few active stars but always with $EW(H\alpha) < 10 \text{ \AA}$ taken here as benchmark. In a sentence, given the low metallicity and old age of 47Tuc, $H\alpha$ emission from CA is expected, if anything, to be smaller than that from Pop I younger counterparts (see also Gizis et al. 2002).

The stars that we selected as bona-fide $H\alpha$ emitters fall in the F0 to M5 spectral range and all show EW larger than $\sim 10 \text{ \AA}$. It is interesting to note that most of the mentioned authors use a cutoff of 1.0 \AA as the minimum EW at which one can unambiguously detect emission in an M dwarf. Coupling the intensity of the $EW(H\alpha)$ measured in this paper with the results from the literature previously described suggests that the $H\alpha$ excess emission that we are sampling cannot come from pure CA.

In general, the analysis above allows us to conclude that for most objects with $H\alpha$ excess in Figure 4 (see also Table 2), and certainly for all those with $EW(H\alpha) > 20 \text{ \AA}$, the source of $H\alpha$ excess emission is not CA. These objects could, however, be interacting binaries, in which one star fills its Roche Lobe and matter is being transferred to the companion. We will investigate this hypothesis in more detail in Section 6, but we first look at the optical properties of known interacting binaries in the field covered by our observations.

5 OPTICAL COUNTERPARTS TO KNOWN X-RAY BINARIES

As mentioned in the introduction, H05 have compiled a catalogue of 300 X-ray sources lying in the central regions of 47 Tuc. The catalogue provides precise absolute coordinates for a number of CVs, ABs and other exotica, but a large number of stars in that catalogue still remain unclassified. Proving that some of these stars have an optical counterpart showing $H\alpha$ excess emission would offer new constraints on their nature, since recombination lines are associated with the mass accretion process in CVs and interacting binaries in general (see e.g. Warner 1995).

We, therefore, searched for counterparts to the H05 X-ray sources in our photometric catalogue, looking specifically for objects with $H\alpha$ excess emission (defined as in Section 3) falling within $0'.5$ of the nominal position of the X-ray source, which already take into account bore-sight correction. This is a reasonable radius of tolerance given the astrometric accuracy of the H05 catalogue and the uncertainties on our astrometric solution ($\sim 0'.3$).

Most of the X-ray sources detected by H05 populate the central regions of the cluster, where the high stellar density is more likely to favour encounters and the formation of stellar exotica (e.g.

Knigge et al. 2008). A total of 204 X-ray sources fall inside our FoV, but 181 of them are located within $70''$ of the cluster centre, where crowding is severe in our observations, particularly in the V and I bands. For this reason, we had so far excluded these regions from our analysis (see Section 3), in order to minimise any systematic effects due to photometric incompleteness. However, our goal here is to find as many counterparts as possible to X-ray sources and to characterise their properties, so photometric incompleteness is no longer an issue.

Our search for counterparts to the X-ray sources over the entire FoV revealed a total of 23 candidate matches with $H\alpha$ excess emission. Inside $70''$ of the cluster centre, where the number of bona-fide $H\alpha$ excess emitters is ~ 1000 , there are 181 X-ray sources, of which 20 have an optical counterpart with $H\alpha$ excess emission, or $\sim 10\%$. Outside of $70''$ there are 23 X-ray sources, of which 3 have an optical counterpart, or $\sim 13\%$. All matches are unique, except for one case in which there are two $H\alpha$ excess sources inside the X-ray error circle, with rather similar V and I magnitudes. Note that the relative low fraction ($\sim 10\%$) of matching optical counterparts with $H\alpha$ excess is a consequence of the detection limit of 10 \AA on the value of $\text{EW}(H\alpha)$, mostly imposed by the quality of the adopted data-set (see also the discussion in Section 3). Nevertheless, as shown in Section 4, this limit allows us to exclude objects whose $H\alpha$ emission is dominated by CA. It is therefore possible that a larger fraction of the X-ray sources in the catalogue of H05 have an optical counterpart with $H\alpha$ emission lines and $\text{EW}(H\alpha) < 10\text{ \AA}$ (at least at the time of our observations).

It is important to consider that the luminosity of CVs is affected by long (days) and short (hours) term variability (Verbunt et al. 1999). Interestingly, the X-ray, optical and ultraviolet flux variation during outburst and superoutbursts are often anticorrelated (Wheatley et al. 2003). Moreover, Fender et al. (2009) found an anticorrelation between X-ray continuum luminosity and the $\text{EW}(H\alpha)$ emission line in X-ray binary systems. Therefore, not all objects detected as X-ray sources in the catalogue of H05 need to show $H\alpha$ excess emission in the observations used in this work.

All the X-ray sources with an optical counterpart are indicated with a cross in Figures 3, 4 and 6, and their coordinates, magnitudes, distance from the nominal position of the X-ray emitter and $\text{EW}(H\alpha)$ values are listed in Table 3. Six of these objects are classified by H05 as CVs (W25, W30, W42, W45, W53 and W122), five as ABs (W22, W47, W69, W93, W228), two as qLMXBs (W58 and W125), while the other ten are unclassified X-ray sources (W78, W80, W81, W145, W255, W305, W310, W312, W319 and W328).

In Figure 7 we show the finding charts from our ACS images in the V and $H\alpha$ bands (labelled V-band and Halpha, respectively), for three CVs namely V1 (W42), W25, W45 and the AB W47. A $0''.2$ solid circle shows the location of the $H\alpha$ excess emitters on the ACS images. We compared these objects with the finding charts in the F336W (U) and F555W (V) bands from the WFPC2 observations of Edmonds et al. (2003a). While these images confirm the accuracy of our astrometric solution, it is interesting to notice that, thanks to the higher spatial resolution of the ACS, we identify as candidate optical counterpart to W45 an object that was not resolved in the photometry of Edmonds et al. (2003a).

As Figure 4 shows, the distribution of $\text{EW}(H\alpha)$ as a function of spectral type for X-ray sources with $H\alpha$ excess agrees well with that of other objects with $H\alpha$ excess that we identified and that are not detected in the X-rays. It is, therefore, possible that the two classes of sources correspond to objects of similar types.

In Figure 6 we show the positions of the stars with $H\alpha$ excess emission and $\text{EW}(H\alpha) > 20\text{ \AA}$ in the $V_0, (V - I)_0$ CMD, using the

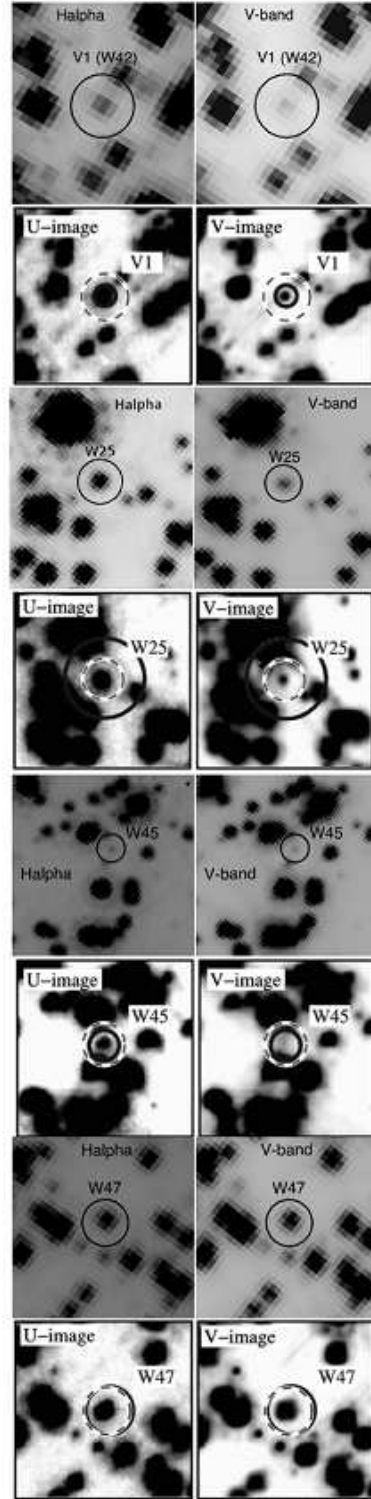


Figure 5. Comparison of HST finding charts for 4 optical identifications in common with Edmonds et al. (2003a). For each star, the V and $H\alpha$ finding charts from the present work (labeled V-band and Halpha, respectively) are compared with F555W- and F336W-band images (V-band and U-band, respectively) acquired with the WFPC2. The $0''.2$ solid circles show the location of the $H\alpha$ excess emitters on our ACS images. The solid circles on the U and V WFPC2 frames show the 4σ uncertainty on the X-ray positions, while the dashed circles show the candidate optical counterparts.

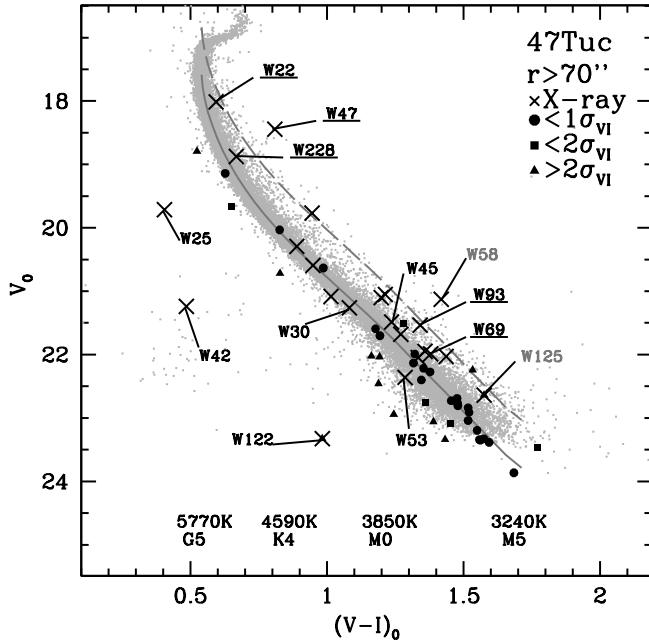


Figure 6. The stars with H α excess emission and $\text{EW}(\text{H}\alpha) > 20\text{\AA}$ are shown as black symbols in the CMD of the cluster. Crosses mark the optical counterparts to X-ray sources across the whole field of view, whereas the grey data points and the H α excess sources marked with solid circles, squares and triangles are located outside a $70''$ radius. The MS mean ridge line (grey solid line) and the spectral types are also shown. The 6 CVs (black characters), the 5 ABs (underlined characters) and the 2 LMXBs (grey characters) are explicitly labelled. The MS ridge line and the location of the equal-mass binary sequence are shown with a solid and dashed line, respectively.

same symbols as in Figure 3. All cluster stars lying at a distance $r > 70''$ from the cluster center are shown in light grey while the 6 CVs, the 5 ABs and the 2 qLMXBs are explicitly labelled. The spectral types derived from the atmospheric models of Bessell et al. (1998) are also shown.

A photometrically unresolved binary system appears as a single star with a flux equal to the sum of the fluxes of the two components. Thus, the MS ridge line (solid line in Figure 6) in practice indicates the location at which the luminosity (and hence mass) of the secondary component is negligible with respect to the primary. The dashed line in Figure 6 shows the location of binary systems where the masses of the two stars are equal and the magnitude of the binary system is 0.752 mag brighter than that of the single star alone. These boundaries allow us to constrain the location of unresolved binaries in the cluster.

As discussed in Section 3, the number of excess emitters increases with spectral type. In Section 4 we explored the possibility that this can be a sign of unusually strong CA. Even if evidence of increased CA in old M dwarfs in wide binary systems with a WD are reported in the literature (see Silvestri et al. 2005), the majority of targets with $\text{EW}(\text{H}\alpha)$ are in the range between 20\AA and 100\AA and can not be linked to purely chromospherically active stars.

An obvious alternative explanation is that these stars are compact binaries actively interacting that were not detected in previous studies. This conclusion seems to be supported by the fact that in the CMD most of these stars are located in the area between the MS ridge line (solid line) and the line identifying the location of equal-

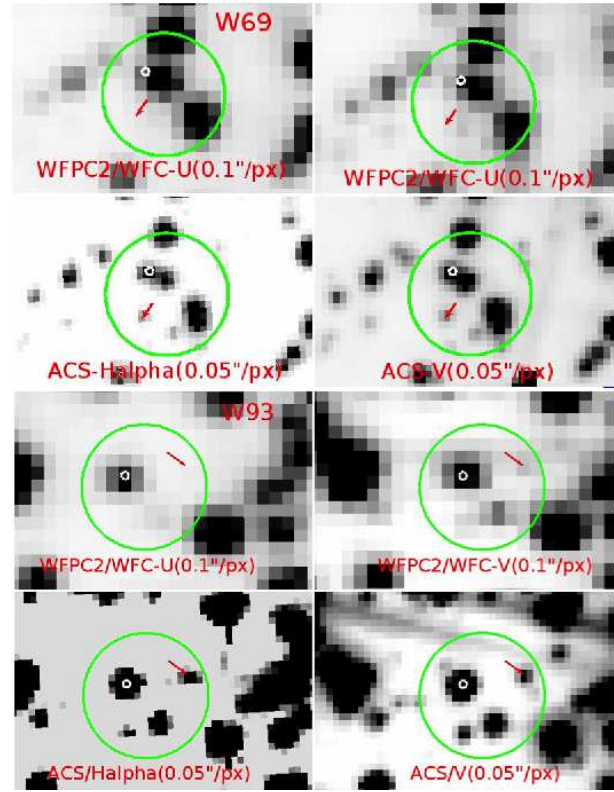


Figure 7. Comparison of the FCs for the optical identifications of two X-ray objects. A large circles (green in the electronic version) of $0.5''$ radius around the nominal position of the X-ray candidate are shown, the small white circles show the published positions of the counterparts, while the small arrow (red in the electronic version) indicates the location of the H α excess emitters.

mass binaries (dashed line). This area is where unresolved MS binaries or BY Draconis stars are expected (e.g. Albrow et al. 2001) and where almost all the stars showing X-ray emission and identified as active binaries by H05 are located. Furthermore, this region may also be populated by Algol-type binaries, which are known to undergo rapid H α emission variations (see Olson & Etzel 1995).

Even though a detailed discussion of the nature of individual objects goes beyond the purpose and scope of the present work, sources W22, W228, W47, W93, and W69 deserve some discussion. W47 is classified by Albrow et al. (2001) as a semidetached W UMa binary with a period of 0.5 days. Hence, a mass transfer stream, and a H α excess emission, should be expected in this case. On the other hand, W 228 is classified as a contact W UMa binary, W 93 as a 4-day eclipsing binary, W 69 as a 3.1-day BY Dra binary, while W 22 is a 2.5-day binary; none of these are likely to be engaged in mass transfer. Nevertheless the H α excess emission that we find makes these objects candidate systems actively undergoing mass transfer.

It is interesting to note that the objects mentioned above fall on the WF detectors of the WFPC2 camera in the observations used by Albrow et al. (2001), Edmonds et al. (2003a) and H05. These detectors offer a plate-scale of $0.1'' \text{ px}^{-1}$, i.e. half of the resolution allowed by the ACS camera used in this work.

For example, as shown in Figure 7 by visually comparing the two data-sets we have realized that inside a $0.5''$ circle around the X-ray for W69 and W93 the objects with H α excess emission (red arrows in the figure) are not the same candidate optical counterparts

proposed by the cited authors (white circles). Indeed, while these objects with $H\alpha$ excess are clearly resolved in the ACS images, they are either blended with nearby stars or too faint to be detected in the WFPC2 images.

We performed a test in order to quantify the probability to obtain false matching from the comparison of the X-ray source catalogue and the list of $H\alpha$ excess emitters. The test simply consists in applying an offset of few arc-seconds to the coordinates of the X-ray sources. We performed the search for optical counterpart among the list of $H\alpha$ emitters following the same strategy described in Section 5. We first performed this test for the stars outside of $70''$ from the cluster centre, where there are 23 X-ray sources and 59 sources with $H\alpha$ excess emission in our catalogue. We offset the catalogue of X-ray stars by $1''$, $2''$ and $3''$ and we did not find any match within $0'.5$. Thus, outside of $70''$ we expect no false matches. We then repeated this test for stars within $70''$ of the cluster centre, where the density of sources is higher and there are 180 X-ray sources and about 1000 stars with $H\alpha$ excess emission at the 5σ level. Given the higher density of objects in these regions, compared with the outskirts of the cluster, if we offset one of the catalogues we do find some false matches. For offsets ranging from $1''$ to $5''$ we find typically 7 matches, of which however only typically 3 within a $0'.3$ search radius. We therefore conclude that, in the worst scenario, 7 false matches should be expected among the 20 matches.

Non-periodic strong variability would also offer an explanation to the unusual location of stars W 47 (AB) and W 58 (qLX). W 47 shows clear signs of variability in the Chandra observations, as reported by H05 (see their Figure 6). The same authors identify W 47 with an optical variable, corresponding to object number 8 in the list of Edmonds et al. (1996) and PC1–V08 in that of Albrow et al. (2001). Star W 58 is also classified as variable by H05 and Edmonds et al. (2003a). While the finding charts shown in Figure 7 demonstrate the good match in our source identification, the location of these two stars on the CMD is not in agreement with the one reported by Edmonds et al. (1996) and Albrow et al. (2001). However, as a consistency check of our photometric measurements, we have looked for these objects in the photometric catalogue of the same region provided as part of the ACS Globular Cluster Treasury programme (Sarajedini et al. 2007)³. The magnitudes that we measured in the V (F606W) and I (F814W) bands are fully consistent with those of the ACS Globular Cluster Treasury programme. We conclude, therefore, that our photometry is correct and that these two sources are likely to be affected by episodes of large variability (we show in Table 3 the timescale of the variability at the 99% and 99.9% confidence levels as derived by H05).

Stars with $H\alpha$ excess in the colour range $1 < (V-I)_0 < 1.5$ and lying away from the MS ridge line by more than twice their colour uncertainty σ_{VI} represent a rather interesting sub-class of objects. These stars, indicated by solid triangles in Figure 6, have $EW(H\alpha)$ in the range between $\sim 20 \text{ \AA}$ and $\sim 130 \text{ \AA}$ suggesting that they are accretors. These stars systematically populate the bluest side of the MS, far from the location of binary stars. Since a CV showing X-ray and $H\alpha$ emission, namely W53, is located in the same region of the CMD, we conclude that these objects too are indeed most likely candidate CVs.

6 DISCUSSION AND CONCLUSIONS

The CMD is often used to constrain the nature of X-ray sources in a GC (e.g. Cohn et al. 2010). In a study devoted to the detection of CVs in the GC NGC 6752, Bailyn et al. (1996, hereafter B96) identified two CVs from their $H\alpha$ and UV excess using observations with the WFPC2 camera on board the HST. These authors notice that the location of these stars in the vicinity of the MS in the $V, V-I$ CMD (the same location as occupied by our candidates; see also their Figure 3) is not typical for CVs. B96 suggest that the red colours of the counterpart may indicate that there is a significant contribution from a low-mass secondary to the optical emission from the source.

The $EW(H\alpha)$ values that we have measured for these objects strongly support the hypothesis that they are bona-fide CVs. Pretorius & Knigge (2008) used observations from the AAO/UKST SuperCOSMOS $H\alpha$ Survey (SHS; Parker et al. 2005) to identify CVs through their $H\alpha$ emission. They found 16 CVs with spectroscopically measured $EW(H\alpha)$ in the range between $\sim 20 \text{ \AA}$ and $\sim 130 \text{ \AA}$, in excellent agreement with the values we obtained for the 6 CVs with X-ray and $H\alpha$ emission (see Table 3) and with the measured $EW(H\alpha)$ of the candidate CVs (see Figures 3 and 4).

This finding opens up an interesting new scenario. Theoretical models for CV formation in GCs predict that a cluster like 47 Tuc should harbor ~ 200 CVs, most of which should have formed dynamically (Di Stefano & Rappaport 1994; Ivanova et al. 2006; Pooley & Hut 2006). About 50% of these objects are expected to reside in the cluster core. The combined observational effort described by H05 and Knigge et al. (2008), including all the detections obtained at X-ray, optical and UV wavelengths, together with spectroscopy from the HST, bring the total number of candidate CVs detected so far in 47 Tuc to ~ 100 CVs. Our observations suggest that this number is likely to grow and might approach the level predicted by theoretical models.

Let us assume that the density distribution of these known CV candidates is representative of the radial distribution of the entire population of CVs in 47 Tuc. A total of 15 of the X-ray CVs are located inside the core radius ($\sim 21''$; Mapelli et al. 2004), while only 2 are found outside of $70''$. Our selection based on $H\alpha$ excess emission in the region outside of $70''$, reveals 12 objects with $EW(H\alpha) > 20 \text{ \AA}$ and showing a $(V-I)_0$ colour at least $> 1\sigma_{VI}$ bluer than the MS ridge line (solid black squares and triangles in Figure 6). We include also the X-ray source W 122, classified as a CV by H05. Under the assumption that the ratio of $H\alpha$ and X-ray emitters is constant and of order 6 everywhere, we should expect to detect ~ 90 CVs with $H\alpha$ emission inside the core radius, a number in full agreement with the theoretical expectations. Therefore, by allowing an efficient detection of candidate CVs, our method is able to reconcile theoretical expectation with observations.

It is appropriate to point out that the validity of the observational approach presented in this paper was already exploited by Witham et al. (2006, hereafter W06). These authors used observations from the Isaac Newton Telescope Photometric $H\alpha$ Survey of the northern galactic plane (IPHAS) to study the $H\alpha$ emission of 71 known CVs. The selection strategy presented in our paper is quite similar to the one adopted in W06, with the difference that we use the V band instead of the r' filter to estimate the stellar continuum below the $H\alpha$ line. The advantage of our approach are described in Section 3. Nevertheless, it is comforting that W06 report a 70% recovery rate of known CVs as $H\alpha$ emitters and that they do not find statistically significant dependence of the recovery rate of CVs via their $H\alpha$ emission on the actual CV type.

³ The catalogue is available online at http://www.astro.ufl.edu/ata/public_hstgc/databases.html.

An important result of this study is that chromospheric activity alone is not sufficient to produce $H\alpha$ excess emission with $EW(H\alpha) > 20 \text{ \AA}$ and that the origin of such a strong emission has to be associated with mass accretion. This is crucial for the identification and study of not only interacting binaries but also of T Tauri stars in star forming regions. Our results show that the method developed by DM10 to derive $EW(H\alpha)$ from a suitable combination of photometry in the $H\alpha$, V and I bands can effectively distinguish stars undergoing mass accretion from chromospherically active objects.

ACKNOWLEDGMENTS

We are very grateful to an anonymous referee for the constructive comments and useful suggestions that have helped us to improve the overall presentation of the scientific results. The authors thank Paolo Montegriffo for his help with the CataXcorr software package. The research leading to these results has received funding from the European Community's Seventh Framework Programme (/FP7/2007-2013/) under grant agreement No 229517.

REFERENCES

- Albrow, M. D., Gilliland, R. L., Brown, T. M., et al. 2001, *ApJ*, 559, 1060
- Anderson, J., Piotto, G., King, I. R., Bedin, L. R., & Guhathakurta, P. 2009, *ApJL*, 697, L58
- Anderson, J., & Bedin, L. R. 2010, *PASP*, 122, 1035
- Appenzeller, I., & Mundt, R. 1989, *A&ARv*, 1, 291
- Bailyn, C. D. 1995, *ARA&A*, 33, 133
- Bailyn, C. D., Rubenstein, E. P., Slavin, S. D., et al. 1996, *ApJL*, 473, L31
- Baraffe, I., Chabrier, G., Allard, F., & Hauschildt, P. H. 1997, *A&A*, 327, 1054
- Bassa, C. G., Pooley, D., Verbunt, F., et al. 2008, *A&A*, 488, 921
- Beccari, G., et al. 2010, *ApJ*, 720, 1108
- Bertin, E., & Arnouts, S. 1996, *A&AS*, 117, 393
- Bertout, C. 1989, *ARA&A*, 27, 351
- Bessell, M. S., Castelli, F., & Plez, B. 1998, *A&A*, 333, 231
- Camilo, F., Lorimer, D. R., Freire, P., Lyne, A. G., & Manchester, R. N. 2000, *ApJ*, 535, 975
- Cardelli, J. A., Clayton, G. C., & Mathis, J. S. 1989, *ApJ*, 345, 245
- Carretta, E., Gratton, R. G., Lucatello, S., Bragaglia, A., & Bonifacio, P. 2005, *A&A*, 433, 597
- Carretta, E., Bragaglia, A., Gratton, R., D'Orazi, V., & Lucatello, S. 2009, *A&A*, 508, 695
- Cohn, H. N., Lugger, P. M., Couch, S. M., et al. 2010, *ApJ*, 722, 20
- De Marchi, G., Panagia, N., & Romaniello, M. 2010, *ApJ*, 715, 1 (DM10)
- De Marchi, G., Panagia, N., Romaniello, M., et al. 2011, *ApJ*, 740, 11
- Di Stefano, R., & Rappaport, S. 1994, *ApJ*, 423, 274
- Edmonds, P. D., Gilliland, R. L., Guhathakurta, P., et al. 1996, *ApJ*, 468, 241
- Edmonds, P. D., Gilliland, R. L., Heinke, C. O., & Grindlay, J. E. 2003a, *ApJ*, 596, 1177
- Edmonds, P. D., Gilliland, R. L., Heinke, C. O., & Grindlay, J. E. 2003b, *ApJ*, 596, 1197
- Fender, R. P., Russell, D. M., Knigge, C., et al. 2009, *MNRAS*, 393, 1608
- Ferraro, F. R., D'Amico, N., Possenti, A., Mignani, R. P., & Paltrinieri, B. 2001, *ApJ*, 561, 337
- Ferraro, F. R., Beccari, G., Rood, R. T., et al. 2004, *ApJ*, 603, 127
- Gizis, J. E., Reid, I. N., & Hawley, S. L. 2002, *AJ*, 123, 3356
- Grindlay, J. E., Heinke, C., Edmonds, P. D., & Murray, S. S. 2001, *Science*, 292, 2290
- Harris, W. E. 1996, *AJ*, 112, 1487
- Hawley, S. L., Gizis, J. E., & Reid, I. N. 1996, *AJ*, 112, 2799
- Hawley, S. L., Reid, I. N., & Tourtellot, J. G. 2000, *Very Low-Mass Stars and Brown Dwarfs*, 109
- Heinke, C. O., Grindlay, J. E., Edmonds, P. D., et al. 2005, *ApJ*, 625, 796 (H05)
- Ivanova, N., Heinke, C. O., Rasio, F. A., et al. 2006, *MNRAS*, 372, 1043
- Kafka, S., & Honeycutt, R. K. 2006, *AJ*, 132, 1517
- Kalirai, J. S., Richer, H. B., Anderson, J., et al. 2012, *AJ*, 143, 11
- Koenigl, A. 1991, *ApJL*, 370, L39
- Knigge, C., Zurek, D. R., Shara, M. M., & Long, K. S. 2002, *ApJ*, 579, 752
- Knigge, C., Dieball, A., Maíz Apellániz, J., et al. 2008, *ApJ*, 683, 1006
- Knigge, C., Baraffe, I., & Patterson, J. 2011, *ApJS*, 194, 28
- Kong, A. K. H., Bassa, C., Pooley, D., et al. 2006, *ApJ*, 647, 1065
- Linsky, J. L., & Ayres, T. R. 1978, *ApJ*, 220, 619
- Linsky, J. L. 1980, *ARA&A*, 18, 439
- Lu, T.-N., Kong, A. K. H., Verbunt, F., et al. 2011, *ApJ*, 736, 158
- Lyra, W., & Porto de Mello, G. F. 2005, *A&A*, 431, 329
- Mapelli, M., Sigurdsson, S., Colpi, M., et al. 2004, *ApJL*, 605, L29
- Milone, A. P., Piotto, G., Bedin, L. R., et al. 2011, *arXiv:1111.0552*
- Olson, E. C., & Etzel, P. B. 1995, *AJ*, 109, 1308
- Pace, G., & Pasquini, L. 2004, *A&A*, 426, 1021
- Pallanca, C., Dalessandro, E., Ferraro, F. R., et al. 2010, *ApJ*, 725, 1165
- Pallanca, C., Dalessandro, E., Ferraro, F. R., Lanzoni, B., & Beccari, G. 2013, *ApJ*, 773, 122
- Parker, Q. A., Philipps, S., Pierce, M. J., et al. 2005, *MNRAS*, 362, 689
- Pasquini, L., & Pallavicini, R. 1991, *A&A*, 251, 199
- Pasquini, L., & Lindgren, H. 1994, *A&A*, 283, 179
- Pooley, D., Lewin, W. H. G., Homer, L., et al. 2002, *ApJ*, 569, 405
- Pooley, D., & Hut, P. 2006, *ApJL*, 646, L143
- Pretorius, M. L., & Knigge, C. 2008, *MNRAS*, 385, 1471
- Rocha-Pinto, H. J., Castilho, B. V., & Maciel, W. J. 2002, *A&A*, 384, 912
- Sarajedini, A., Bedin, L. R., Chaboyer, B., et al. 2007, *AJ*, 133, 1658
- Schmidt, S. J., Cruz, K. L., Bongiorno, B. J., Liebert, J., & Reid, I. N. 2007, *AJ*, 133, 2258
- Sicilia-Aguilar, A., Henning, T., Kainulainen, J., & Roccatagliata, V. 2011, *ApJ*, 736, 137
- Shu, F. H., Najita, J., Ruden, S. P., & Lizano, S. 1994, *ApJ*, 429, 797
- Silvestri, N. M., Hawley, S. L., & Oswalt, T. D. 2005, *AJ*, 129, 2428
- Sirianni, M., et al. 2005, *PASP*, 117, 1049
- Spezzi, L., De Marchi, G., Panagia, N., Sicilia-Aguilar, A., & Ercolano, B. 2011, *MNRAS*, in press, *arXiv:1111.0835*
- Stetson, P. B. 1987, *PASP*, 99, 191

- Stetson, P.B., 1994, *PASP*, 106, 250
- Verbunt, F., Wheatley, P. J., & Mattei, J. A. 1999, *A&A*, 346, 146
- Warner, B. 1995, *Cataclysmic variable stars*, Cambridge Astrophysics Series, Cambridge: Cambridge University Press
- West, A. A., Hawley, S. L., Walkowicz, L. M., et al. 2004, *AJ*, 128, 426
- Wheatley, P. J., Mauche, C. W., & Mattei, J. A. 2003, *MNRAS*, 345, 49
- White, R. J., & Basri, G. 2003, *ApJ*, 582, 1109
- Williams, G. 1983, *ApJS*, 53, 523
- Witham, A. R., Knigge, C., Gänsicke, B. T., et al. 2006, *MNRAS*, 369, 581
- Zhao, J. K., Oswalt, T. D., Rudkin, M., Zhao, G., & Chen, Y. Q. 2011, *AJ*, 141, 107

Table 2: Candidate H α excess emitters.

Name	RA	Dec	V	I	H α	EW(H α) [\AA]
1	00:24:06.82	-72:06:09.87	18.546	17.952	18.010	13.74 \pm 1.60
2	00:24:17.71	-72:05:33.38	18.907	18.344	18.233	27.12 \pm 2.13
3	00:24:12.44	-72:06:11.22	19.255	18.589	18.196	63.91 \pm 1.41
4	00:24:18.35	-72:06:14.64	19.644	18.850	18.977	15.47 \pm 1.41
5	00:24:17.50	-72:05:35.26	19.673	18.915	19.021	15.99 \pm 1.43
6	00:23:49.91	-72:04:11.30	19.770	19.081	19.011	29.15 \pm 2.03
7	00:24:15.86	-72:05:56.50	20.147	19.281	19.203	37.43 \pm 2.29
8	00:24:20.37	-72:05:35.68	20.299	19.392	19.607	12.34 \pm 1.50
9	00:23:54.62	-72:06:07.68	20.709	19.721	19.994	10.83 \pm 1.34
10	00:24:21.07	-72:05:28.60	20.748	19.722	19.813	28.26 \pm 1.56
11	00:23:58.48	-72:06:30.11	20.833	19.966	19.803	46.63 \pm 2.21
12	00:23:45.94	-72:03:46.16	20.944	19.873	20.178	11.57 \pm 1.50
13	00:23:46.94	-72:05:27.25	21.139	20.044	20.355	12.06 \pm 1.50
14	00:23:43.70	-72:04:42.17	21.248	20.115	20.398	15.93 \pm 1.67
15	00:24:21.43	-72:04:15.97	21.353	20.356	20.608	12.86 \pm 1.86
16	00:24:18.93	-72:04:17.59	21.517	20.279	20.647	13.35 \pm 1.55
17	00:23:55.54	-72:06:29.16	21.627	20.307	20.556	27.52 \pm 2.64
18	00:23:52.64	-72:03:59.05	21.708	20.491	20.763	20.56 \pm 1.81
19	00:23:51.79	-72:06:03.40	21.816	20.583	20.743	31.75 \pm 2.52
20	00:24:19.70	-72:04:09.27	21.997	20.760	21.120	13.96 \pm 1.77
21	00:23:45.70	-72:04:27.72	22.106	20.745	21.033	25.86 \pm 2.03
22	00:23:49.52	-72:05:38.62	22.136	20.934	20.468	112.23 \pm 1.10
23	00:23:52.34	-72:05:43.39	22.150	20.918	21.169	23.12 \pm 2.16
24	00:23:55.61	-72:06:00.78	22.212	20.840	21.252	15.46 \pm 1.83
25	00:23:54.57	-72:05:49.39	22.227	20.933	21.287	16.92 \pm 1.72
26	00:24:20.41	-72:04:59.93	22.247	20.664	21.141	19.06 \pm 1.73
27	00:23:47.23	-72:05:34.88	22.248	20.892	21.149	28.54 \pm 2.22
28	00:23:47.71	-72:04:49.64	22.310	20.986	21.347	17.65 \pm 2.02
29	00:23:46.51	-72:05:31.92	22.331	20.938	21.294	21.20 \pm 2.11
30	00:23:46.18	-72:03:47.22	22.357	20.784	21.205	23.59 \pm 2.76
31	00:23:51.23	-72:05:23.88	22.387	20.970	21.250	29.37 \pm 1.96
32	00:24:01.62	-72:06:02.79	22.448	20.982	21.437	15.92 \pm 1.79
33	00:23:53.19	-72:05:35.48	22.515	21.130	21.474	21.90 \pm 1.71
34	00:23:52.18	-72:03:48.37	22.571	21.343	21.517	30.14 \pm 1.94
35	00:23:51.85	-72:05:28.97	22.620	21.172	21.575	19.57 \pm 2.20
36	00:23:53.97	-72:03:50.22	22.754	21.139	21.531	28.18 \pm 1.65
37	00:23:43.75	-72:04:32.68	22.804	21.288	21.173	82.34 \pm 1.21
38	00:24:23.96	-72:05:13.79	22.843	21.348	21.748	21.96 \pm 1.83
39	00:23:48.33	-72:05:16.16	22.866	21.467	20.345	301.35 \pm 0.50
40	00:24:06.40	-72:06:26.63	22.882	21.474	21.868	18.56 \pm 2.12
41	00:23:47.93	-72:04:20.71	22.884	21.366	21.770	22.65 \pm 2.11
42	00:24:01.21	-72:05:58.79	22.907	21.430	21.843	20.00 \pm 2.10
43	00:23:50.11	-72:04:09.17	22.920	21.401	21.547	48.89 \pm 1.68
44	00:24:01.58	-72:06:03.14	22.923	21.316	21.799	19.55 \pm 2.05
45	00:24:04.39	-72:06:01.84	22.954	21.398	21.776	26.78 \pm 2.09
46	00:23:58.23	-72:06:22.33	23.025	21.465	21.871	24.37 \pm 2.29
47	00:24:19.86	-72:05:50.88	23.057	21.773	22.071	21.33 \pm 2.30
48	00:23:52.06	-72:05:52.25	23.154	21.598	21.573	72.52 \pm 1.44
49	00:24:02.22	-72:06:12.22	23.174	21.745	22.098	23.14 \pm 2.36
50	00:23:47.83	-72:05:43.70	23.202	21.711	21.937	38.60 \pm 2.26
51	00:24:19.30	-72:05:41.18	23.310	21.721	22.106	27.65 \pm 2.30
52	00:24:03.84	-72:06:21.71	23.441	22.419	21.779	127.08 \pm 1.08
53	00:23:55.24	-72:05:44.63	23.442	21.828	20.658	359.66 \pm 0.45
54	00:24:22.34	-72:04:11.02	23.453	21.981	20.725	365.81 \pm 0.48
55	00:23:55.32	-72:05:53.33	23.455	21.857	22.257	26.65 \pm 2.33
56	00:23:50.78	-72:04:07.57	23.467	21.866	22.000	55.04 \pm 1.63
57	00:24:12.62	-72:06:08.16	23.499	21.866	21.462	141.46 \pm 0.93
58	00:23:51.60	-72:05:51.52	23.574	21.762	22.122	40.24 \pm 2.23

Continued on next page

Name	RA	Dec	V	I	H α	EW(H α) [\AA]
59	00:24:21.68	-72:05:46.24	23.979	22.255	20.707	569.99 ± 0.36

Table 3. Objects with X-ray emission from the catalogue of H05 showing H α excess emission. We use the names of the sources as given by H05 in their Table 2.

Name	RA	Dec	V	I	H α	EW(H α) [\AA]	distance [arcsec]	classification*
W25	00:24:07.131	-72:05:45.85	19.830	19.386	19.256	23.05 \pm 1.20	0.07	CV (D)
W45	00:24:03.762	-72:04:22.82	21.601	20.325	20.560	26.69 \pm 1.92	0.16	CV (DH)
W30	00:24:05.991	-72:04:56.24	21.378	20.257	20.235	44.75 \pm 2.47	0.06	CV (DY)
W42	00:24:04.244	-72:04:58.11	21.355	20.831	19.970	124.81 \pm 1.53	0.09	CV (DHY)
W122	00:24:03.840	-72:06:21.71	23.441	22.419	21.779	127.09 \pm 1.08	0.10	CV (D)
W53	00:24:02.509	-72:05:10.80	22.474	21.149	21.235	44.42 \pm 2.67	0.46	CV (Y)
W22	00:24:07.822	-72:05:24.44	18.129	17.496	17.633	9.04 \pm 1.19	0.11	AB
W47	00:24:03.452	-72:05:05.35	18.558	17.710	17.925	10.22 \pm 1.24	0.07	AB (DHY)
W69	00:24:12.704	-72:04:22.72	22.105	20.686	20.904	35.61 \pm 1.87	0.46	AB
W228	00:24:18.596	-72:04:55.34	18.989	18.282	18.379	14.96 \pm 1.16	0.25	AB
W93	00:24:12.073	-72:05:07.47	21.650	20.269	20.443	38.11 \pm 1.68	0.38	AB
W58	00:24:00.946	-72:04:53.31	21.243	19.785	19.887	50.38 \pm 1.38	0.11	qLX (DHY)
W125	00:23:53.975	-72:03:50.22	22.754	21.139	21.531	28.18 \pm 1.65	0.15	qLX (D?H)
W319	00:23:58.849	-72:04:47.38	22.061	20.663	21.010	22.24 \pm 2.44	0.37	(H?)
W80	00:24:02.540	-72:04:41.04	19.881	18.896	19.165	11.03 \pm 1.49	0.49	
W312	00:24:00.516	-72:05:17.26	20.407	19.478	19.680	14.24 \pm 1.43	0.41	
W145	00:23:54.625	-72:06:07.68	20.709	19.721	19.994	10.83 \pm 1.34	0.24	
W255	00:24:10.566	-72:04:43.91	21.164	19.911	20.043	35.59 \pm 1.94	0.30	
W78	00:24:03.687	-72:05:22.26	21.197	20.143	20.365	17.72 \pm 1.70	0.30	
W310	00:24:00.819	-72:05:42.77	21.216	19.978	20.353	12.79 \pm 1.75	0.30	
W81	00:24:01.799	-72:05:12.78	21.794	20.484	20.542	46.66 \pm 1.36	0.47	
W328	00:23:56.328	-72:04:37.84	22.144	20.668	20.966	30.57 \pm 2.13	0.47	
W305	00:24:02.003	-72:04:25.47	22.162	20.789	20.975	36.44 \pm 1.68	0.19	

Note. — * Source classification taken from H05; CV = Cataclysmic variables; qLX = low-mass X-ray binaries containing accreting neutron stars; AB = active binaries. The variability timescale of each star and the associated confidence level is indicated in parentheses as follow: D, H and Y for 99.9 % variability confidence on day, hours and years timescale, respectively. D? and H? indicate a 99 % variability confidence level on timescales of days and hours, respectively.